Case Studies in Chemical and Environmental Engineering 10 (2024) 100832

Contents lists available at ScienceDirect

Case Studies in Chemical and Environmental Engineering

journal homepage: www.sciencedirect.com/journal/case-studies-in-chemical-and-environmental-engineering

Case Report

Solvothermal synthesized N–S doped carbon dots derived from cavendish banana peel (*Musa paradisiaca*) for detection of Fe(III) and Pb(II)

Muhammadin Hamid [a,*], Syahrul Humaidi [a], Hadi Wijoyo [a], Isnaeni Isnaeni [b], Indah Revita Saragi [c], Crystina Simanjuntak [c], Noor Haida Mohd Kaus [d], M.M.A. Kechik [e], Agus Nurbillah [a], Yazid Yaakob [e], Tulus Ikhsan Nasution [a]

[a] Department of Physics, Universitas Sumatera Utara, Medan, 20155, Indonesia
[b] Research Center for Photonics, National Research and Innovation Agency, Building 442 KST BJ Habibie, South Tangerang, 15314, Indonesia
[c] Department of Chemistry, Universitas Sumatera Utara, Medan, 20155, Indonesia
[d] School of Chemical Sciences, Universiti Sains Malaysia, 11800, Pulau, Pinang, Malaysia
[e] Department of Physics, Faculty of Science, Universiti Putra Malaysia, Serdang, 43400, Malaysia

ARTICLE INFO

Keywords:
Adsorption capacity
Energy gap
Heavy metal
Nitrogen-sulphur-carbon dots (NS-CDs)
Solvothermal method

ABSTRACT

The synthesis of NS-CDs was carried out using precursors from Cavendish Banana Peel and L-Cysteine as a dopant with the solvothermal method. The characteristics of NS-CDs were analyzed through High-resolution transmission electron microscopy (HR-TEM), X-ray diffractometer (XRD), energy dispersive X-Ray spectroscopy (EDX), X-Ray Fluorescence spectrometer (XRF), X-Ray photoelectron spectroscopy (XPS), UV–Visible spectrophotometer, Photoluminescence, and Atomic Absorption Spectroscopy (AAS). Based on HR-TEM analysis, NS-CDs exhibited a spherical shape (dot) with an average particle size of 2.03 nm. Meanwhile, based on XRD characterization, NS-CDs showed a graphite carbon shape according to the diffraction patterns (002) and (001). Subsequently, XRF and EDX testing revealed that the elemental composition was dominated by carbon (C), nitrogen (N), Sulphur (S), and oxygen (O). Furthermore, in XPS testing, S2p, C1s, N1s, and O1s peaks correlated around 64 eV, 285 eV, 400 eV, and 531 eV respectively. In UV–Vis testing, the energy gap was found to be 5.71 eV (NS-CDs 3:1), 5.46 eV (NS-CDs 3:1), 5.25 eV (NS-CDs 1:1), 5.51 eV (NS-CDs 1:2), and 5.56 eV (NS-CDs 1:3). Characterization of PL for NS-CDs 3:1, 2:1, 1:1, 1:2, 1:3 showed peak excitation at 403 nm and emission at 493.39 nm, 493.65 nm, 494.98 nm, 496.04 nm, and 497.11 nm, respectively. During heavy metal ion detection testing, Fe(III) and Pb(II) using AAS instruments, it was found that the NS-CDs 1:3 sample yielded the best results with an Adsorption capacity worth 21.35 mg/L and Removal Efficiency worth 85.40 %. These results clearly indicate that NS-CDs material can be used as an ideal heavy metal detection material, especially in wastewater.

1. Introduction

Almost all countries, both developing and developed countries, make an important contribution to the industrial sector, such as the textile and mining industries. In recent years, increased industrialization and population have led to urbanization and increased air, water and soil pollution. The availability of clean water is increasingly limited due to the impact of industrial growth, causing water crises around the world, especially in developing countries. The cause of damage to aquatic ecosystems can be organic matter, bacteria, viruses, dyes, and heavy metal ions originating from the residual production of the printing industry, chemical factories, textiles, pharmaceuticals, and electronics. Water pollutants with non-biodegradable properties pose a great risk to human health. One of the most common heavy metal wastes are arsenic (As), cadmium (Cd), chrome (Cr), lead (Pb), copper (Cu), zinc (Zn), iron (Fe), lead (Pb) and so on, which are often found in the textile, metallurgical, agrochemical, and mining industries [1]. Heavy metals are commonly known as high-density metals, which can pose a threat to the environment and cause various diseases [2].

In the modern industrial era, attention to the impact of heavy metal wastes, such as iron (Fe) and lead (Pb) ions, has become increasingly urgent [3]. These two metals, which are often generated from industrial processes and human activities, have the potential to cause serious environmental damage and public health problems. In an effort to

* Corresponding author.
E-mail address: muhammadin.hamid@usu.ac.id (M. Hamid).

https://doi.org/10.1016/j.cscee.2024.100832
Received 23 April 2024; Received in revised form 22 June 2024; Accepted 26 June 2024
Available online 29 June 2024

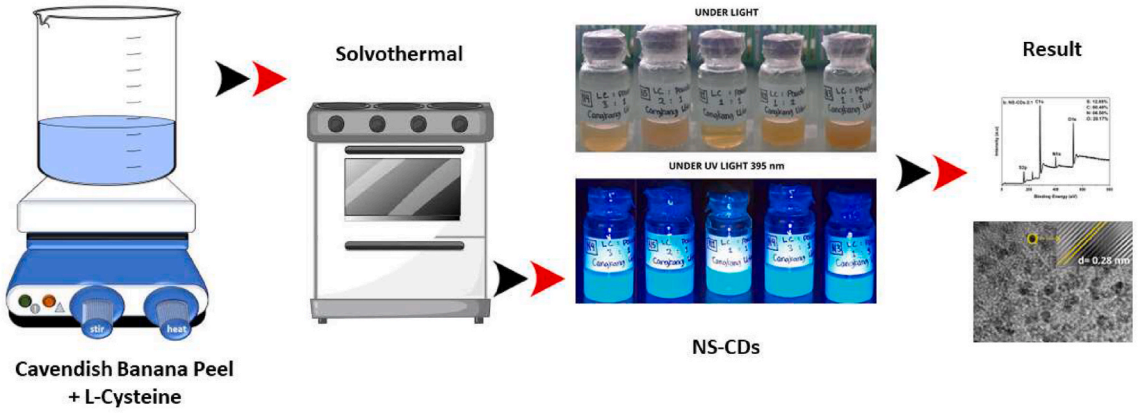

Fig. 1. The method used to the preparation NS-CDs from cavendish banana peels.

understand and address the challenges faced by the presence of these heavy metal wastes, research and innovative actions are becoming increasingly important. There is a need for research to explore the environmental and health impacts of iron and lead heavy metal waste ions, and actions that can be taken to reduce the risks they pose [4]. Identification and prevention are the best measures for environmental protection, so an accurate, fast and affordable method is needed to detect heavy metal effluents. Currently, Fe(II) and Pb(II) detection can be performed using different analytical methods such as mass spectroscopy, coupled plasma spectroscopy, electrochemistry, spectrophotometry, colorimetry, electron paramagnetic resonance (EPR), and Atomic Absorption Spectrophotometry (AAS) [5]. One of the environmentally friendly materials that can be developed into heavy metal ion detectors is carbon dots doped with nitrogen and Sulphur [6].

Carbon dots (CDs) are a new material of fluorescent nanocarbon materials [7]. In the manufacture of carbon dots, each synthesis process and the choice of carbon precursor play an important role in determining the structure of nanocarbon materials along with the degree of carbonization and reaction time [8]. Doping such as nitrogen, Sulphur, and transition metals effectively changes the electronic structure and energy levels of carbon dots which directly increases the intensity of photoluminescence [9]. CDs can be synthesized using autocombustion, hydrothermal, solvothermal and other methods which show excellent fluorescence performance and photobleaching ability. CDs are usually synthesized using natural materials such as coffee, palm oil, pecan and banana peel which have high carbon element sources [10].

Banana is a fruit that is widely distributed and consumed throughout the world. This plant grows in tropical and subtropical regions, one of which is Indonesia [11]. Banana peels are often used as an alternative energy source application for briquette making [12], soap making, metal detection of hazardous substances and so on. In studies conducted by Ref. [13] where banana peels can detect heavy metals such as Fe and Pb. Heavy metals have toxic properties, causing adverse effects on human health and ecosystems even in small doses. Fe metal is a class VIII-B chemical element, while Pb metal is a class II-B chemical element. Fe (iron) metal plays an important role in human health. However, excessive intake can cause adverse effects on humans [14]. Pb (lead) metal is used in many fields including cosmetics, paper, dyes, fluorescent lamps, and on a smaller scale in batteries. The divalent mercury ion has ten electrons filling the 5d energy level, so it has a strong potential to form complexes quickly [15].

Based on this explanation, a sensitive material was designed, namely Nitrogen-Sulphur-Carbon Dots (NS-CDs) synthesized from cavendish banana peel material by solvothermal method to detect Fe and Pb heavy metal ions. The characterization tests carried out are testing the structural properties using High-resolution transmission electron microscopy (HR-TEM), X-ray diffractometer (XRD), energy dispersive X-Ray spectroscopy (EDX), X-Ray Fluoresence spectrometer (XRF), and X-Ray photoelectron spectroscopy (XPS), then testing the optical properties are UV–Visible spectrophotometer and Photoluminescence. Then the Nitrogen-Sulphur-Carbon Dots (NS-CDs) testing stage is carried out against heavy metal ions, namely Fe and Pb using the AAS (Atomic Absorption Spectroscopy) instrument. It is expected that the results obtained can be a reference for the next stage of research.

2. Materials and methods

2.1. Materials

Cavendish Banana Peel were taken from Sumatera Utara Province, Indonesia serve as a doping source for carbon. Hexane (C_6H_{14}) and deionized water were bought from CV. Rudang Jaya, Indonesia. L-Cysteine ($C_3H_7NO_2S$) serve as a doping source for nitrogen and Sulphur, were bought from Merck in Germany.

2.2. Preparation of cavendish banana peel powder

The cavendish banana peels are cleaned using distilled water until the dirt is removed. The banana peels were then dried in the sun for easy crushing for 12 h. It was then pulverized using a herb grinder to get a smaller size. It is then filtered using a 200 mesh sieve and ballmill to get the powder form.

2.3. Synthesis of nitrogen sulphur-doped carbon dots (N-CDs)

NS-CDs were synthesized using the solvothermal method. For the first step, Cavendish banana peel powder and L-cysteine and 5 were mixed in a Teflon autoclave with a composition ratio of (Cavendish banana peel powder:L-cysteine = 3:1, 2:1, 1:1, 1:2, and 1:3). The solution was then heated for 30 minutes at 220 °C. After that the solution was cooled to 30 °C, the precipitated solution was washed with n-hexane, dissolved in DI water and centrifuged at 10.000 rpm for 15 minutes. The supernatant were filtered through filter paper (Whatman Filter Paper 125 mm). For further purification the solutions was dialyzed for 24 h until it reached neutral pH. Then, the supernatant was heated at 100 °C using an oven under vacuum for 24 h until dry powder was obtained and stored in an ampere bottle at normal temperature [16,17]. Then the procedure has also been presented in Fig. 1.

2.4. Quantum yield of CDs

The calculation for the Quantum Yield of CDs value is calculated using the following equation (Eq. (1)) from the literature [18]:

$$QYc = QYs \times \frac{I_C}{I_S} \times \frac{A_S}{A_C} \times \left(\frac{\eta_C}{\eta_S}\right)^2 \quad (1)$$

Table 1
Quantum yield of CDs.

materials	QY (%)
NS-CDs 3:1	12.68
NS-CDs 2:1	6.37
NS-CDs 1:1	5.29
NS-CDs 1:2	2.77
NS-CDs 1:3	2,52
Quinine sulfate	54

Quinine sulfate was chosen as the fluorescence reference (QY = 54 % and η = 1.33), where QY ∼ quantum yield value. I ∼ area integrated photoluminescence intensity, A ∼ absorbance value, and η ∼ refractive index of the solvent. Subscript "c" indicates on CDs and Subscript "s" indicates on Quinine sulfate.

2.5. Characterization

High-resolution transmission electron microscopy (HR-TEM, JEOL-2100 TEM) was performed using a accelerating voltage of 200 kV to characterize the NS-CDs solution's morphology. Energy dispersive X-Ray spectroscopy (EDS, Thermo Scientific Quattr S equipped) at 20 kV accelerating voltage with oxford instruments EDX to characterize the elemental composition of the samples. The particle size of CDs was determined with image J software. X-Ray photoelectron spectroscopy (XPS, Kratos Axis Supra) performed with monochromatic Al-Kα radiation of 1486.6 eV at 150 W for chemical analysis of samples. X-Ray Fluoresence spectrometer (XRF, Shimadzu, XRF-1800, Japan) to characterize the chemical composition analysis of NS-CDs. UV–Visible

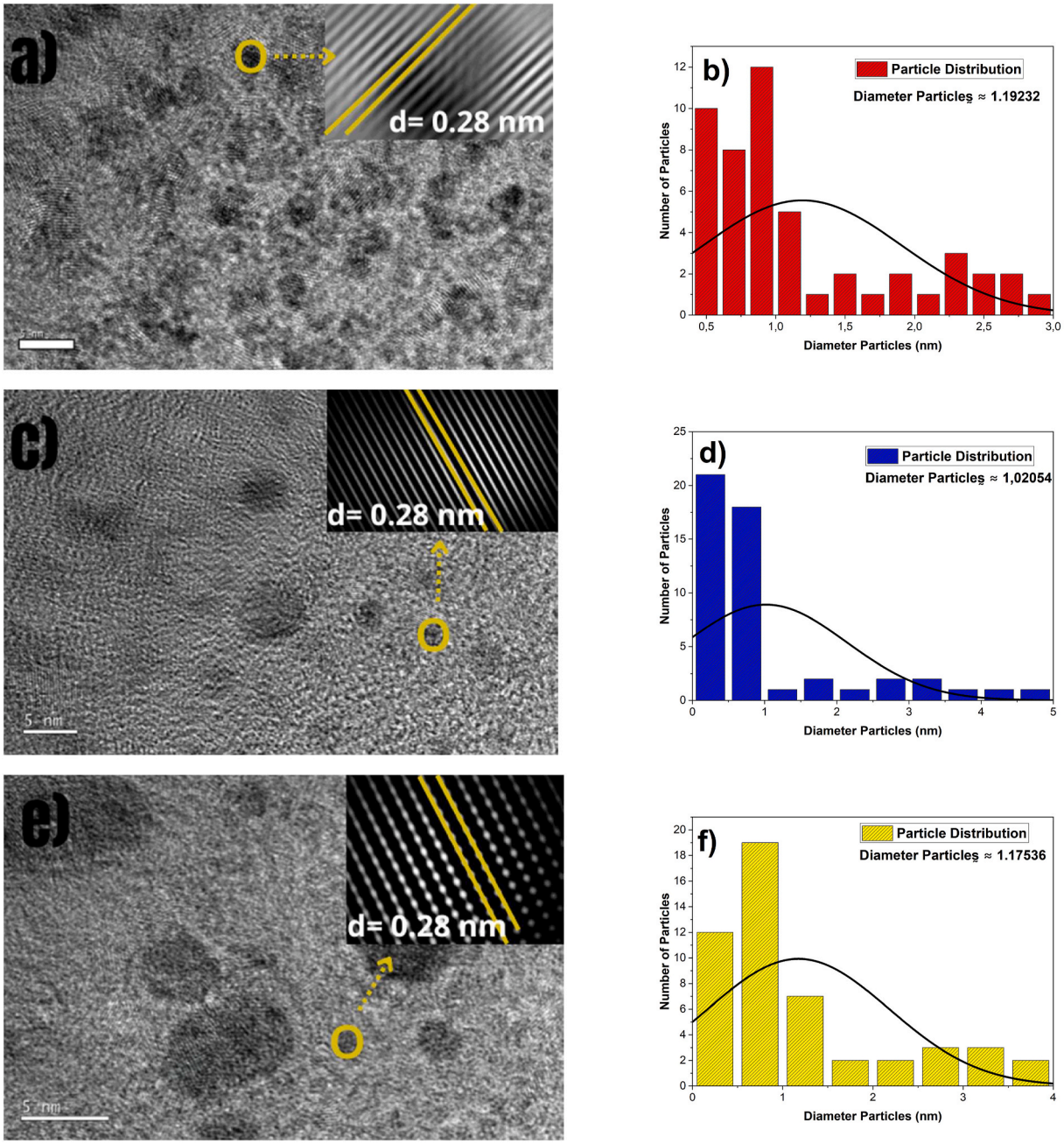

Fig. 2. HR-TEM morphology and lattice spacing of NS-CDs 3:1 (a), NS-CDs 2:1 (c), NS-CDs 1:1 (e), NS-CDs 1:2 (g), NS-CDs 1:3 (i), and Particle size distribution of NS-CDs 3:1 (b), NS-CDs 2:1 (d), NS-CDs 1:1 (f), NS-CDs 1:2 (h), NS-CDs 1:3 (j).

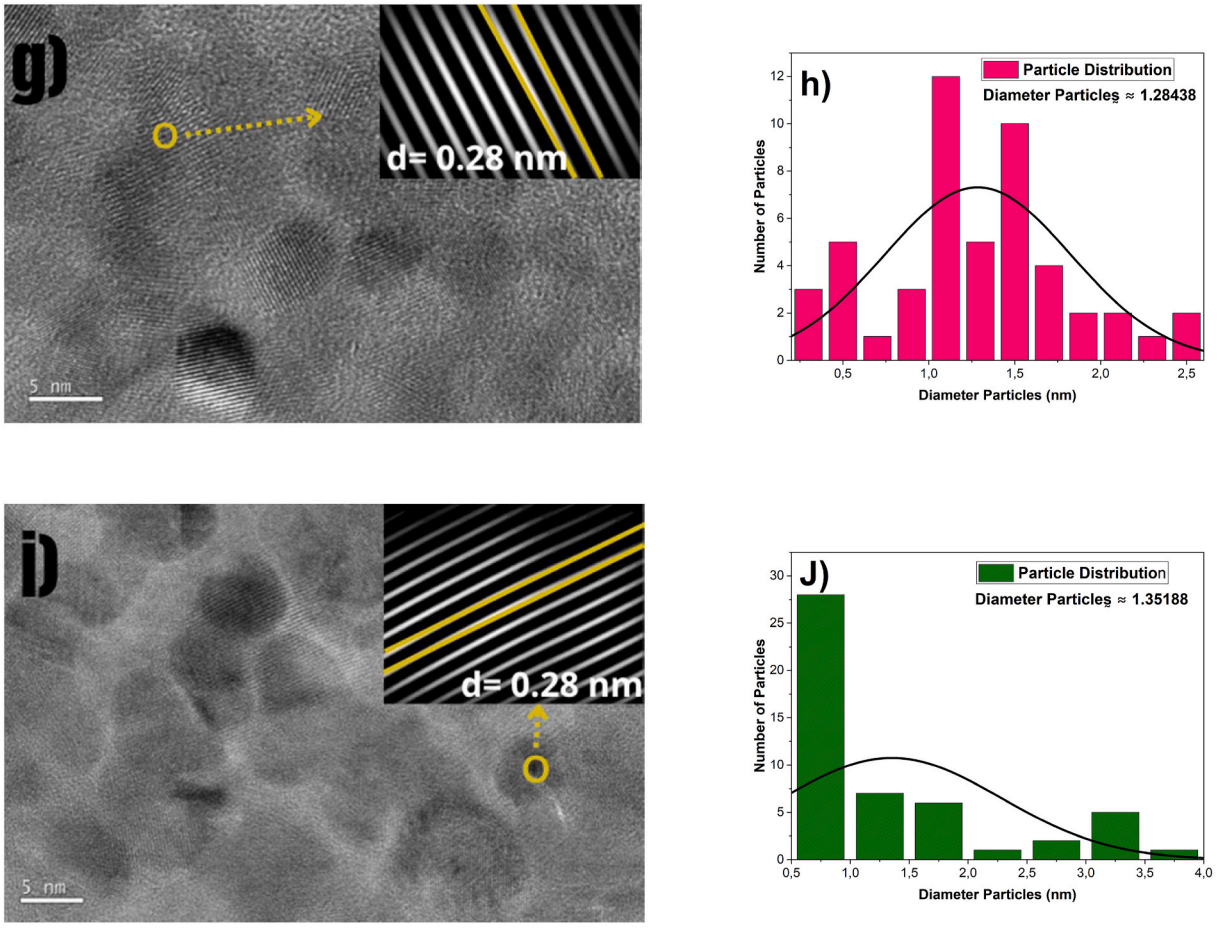

Fig. 2. (*continued*).

spectrophotometer (UV–Vis, Shimadzu UV-1800) in the range 200–700 nm to characterize the UV–vis absorbance spectra. Photoluminescence (UV–Vis, USB2 + F00050 spectrophotometer with 1000 fluorescent) to characterize the PL spectra. X-ray diffractometer (X'pert PRO PANalytical XRD, $\lambda Cu - K\alpha = 1.5406$ Å) to characterize the crystal structure [19].

2.6. Detection of heavy metal ion

The detection of Fe(III) and Pb(II) Ions was evaluated using AAS characterization. AAS (Atomic Absorption Spectroscopy) testing was conducted to determine the adsorption of heavy metals by NS-CDs samples. The AAS testing process in this study includes the preparation of heavy metal waste, the mixing process of heavy metals and NS CDs, and characterization. The overall process can be described as follows:

Each 2.71 g $FeCl_3$ and 2.78 g$PbCl_2$ powder was mixed with 100 ml of distilled water in a beaker. Stirred using a magnetic stirrer for 10 minutes at 500 rpm at room temperature. Furthermore, each variation of NS-CDs powder as much as 0.2 mg was mixed with 5 μL of distilled water. Then the destruction process was carried out by mixing the NS-CDs solution with $FeCl_3$ and $PbCl_2$ powder solutions, then stirring using a magnetic stirrer for 90 minutes. Samples that have been stirred using a magnetic stirrer are then filtered using Whattman 41 filter paper, while separating the sediment in the solution using a permanent magnet. Put each waste into a container that has been prepared then analyze the concentration of heavy metal ions Fe and Pb using AAS.

3. Results and discussion

The characteristics of NS-CDs with various compositions with L-cysteine are described in this section. The QY of NS-CDs respectively, as shown in Table 1.

Based on Table 1, QY decreases gradually with increasing fluorescence intensity. This is related to the photobleaching process, photon induction on diverse functional groups on the surface of the structure and changes in heteroatomic surface groups on the NS-CDs structure [20].

3.1. Structural characterization of synthesized NS–CDs

The morphology and size distribution of NS-CDs were analyzed using HR-TEM which can be seen in Fig. 2. HR-TEM of NS-CDs shown in Fig. 2 shows a spherical shape (dot), small, monodisperse without aggregates and has a size distribution of 0–5 nm. From the calculation of the average particle size of NS-CDs 3:1, 2:1, 1:1, 1:2, 1:3 from Cavendish Banana Peel using image j application are 1.19 nm; 1.02 nm; 1.17 nm; 1.28 nm; 1.35 nm. This shows that the addition of N and S elements can increase the particle size, and both samples are in accordance with the size distribution of nanoscale CDs that have been obtained in the literature [21]. Based on the calculation results using image J software, a lattice spacing of 0.28 nm was obtained from the N-CDs of Fig. 2 (a, c, e, g, i), which is the distance between carbon layers (100) of graphene [22]. This result displays that NS-CDs consist of amorphous and crystalline parts composed of sp2 carbon graphite. Elemental mapping (carbon (C), nitrogen (N), Sulphur (S) and oxygen (O)) of the synthesized NS–CDs are shown in Fig. 3. Consistent with the elemental

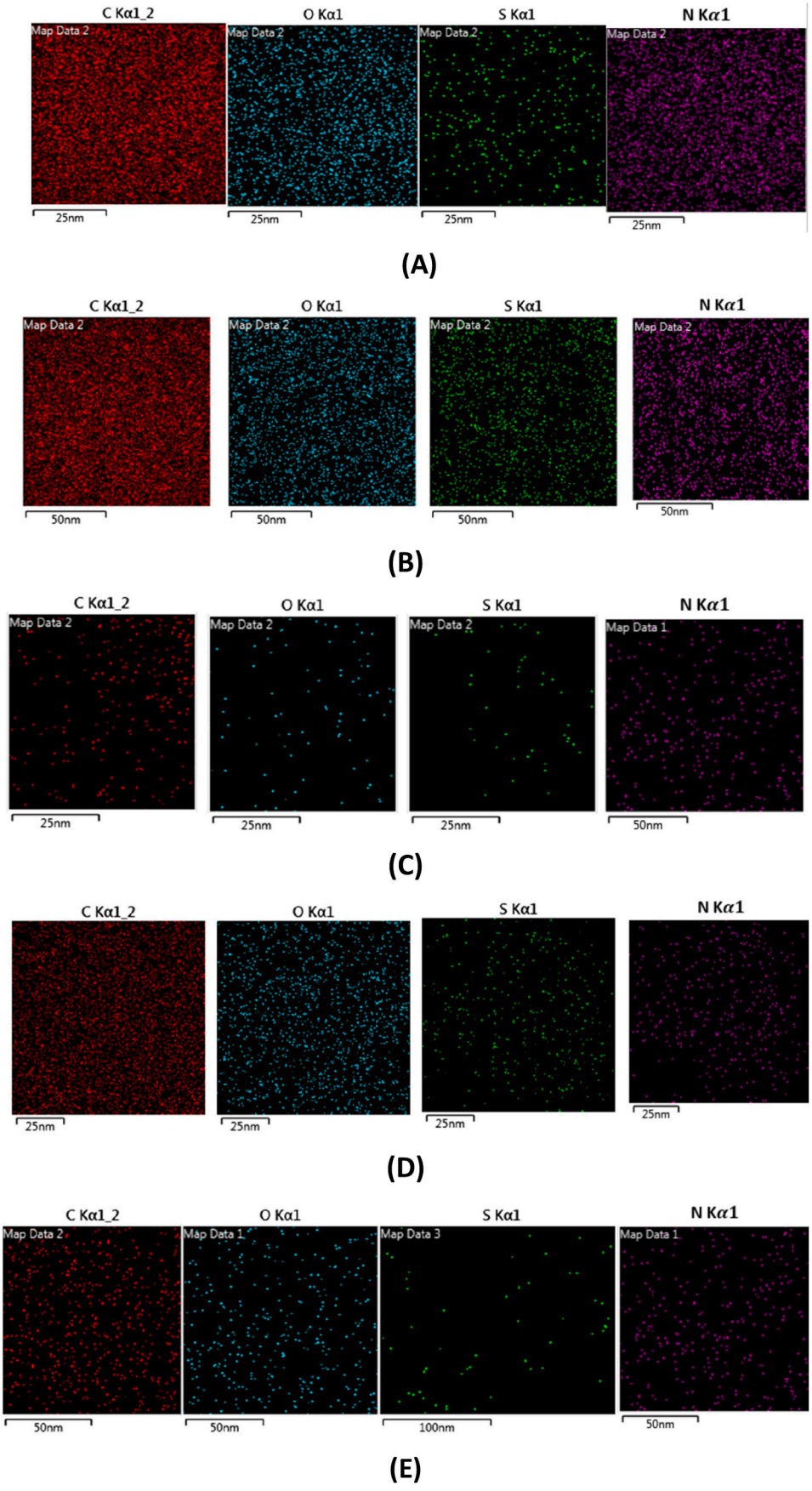

Fig. 3. corresponding elemental mapping images NS-CDs 3:1 (a), NS-CDs 2:1 (b), NS-CDs 1:1 (c), NS-CDs 1:2 (d), NS-CDs 1:3 (e).

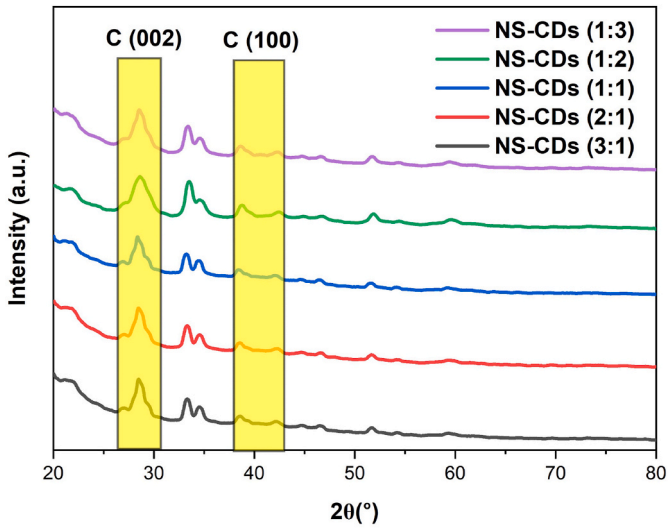

Fig. 4. XRD pattern of the synthesized NS-CDs.

Table 2
Values of some parameters of XRD analysis results.

Parameter	NS-CDs 3:1	NS-CDs 2:1	NS-CDs 1:1	NS-CDs 1:2	NS-CDs 1:3
Grain Size (D)	2.40 nm	2.56 nm	2.40 nm	2.42 nm	2,38 nm
Micro strain (ε)	586.75	581.65	591.91	625.65	572.82
Dislocation (δ)	0.869 nm^{-2}	0.868 nm^{-2}	0.857 nm^{-2}	0.749 nm^{-2}	0.894 nm^{-2}

Table 3
Chemical composition of NS-CDs determined by the Kjeldahl method for N and by XRF analysis.

Element	Weight (%)				
	NS-CDs 3:1	NS-CDs 2:1	NS-CDs 1:1	NS-CDs 1:2	NS-CDs 1:3
C	91.52	95.25	93.08	94,43	86.48
N	4.52	4.07	5.56	4.15	7.67
O	2.93	0.49	0.64	0.67	5.04
S	0.75	0.13	0.21	0.21	0.43
Others (Cl, K, Si, P, Ca and Fe)	0.24	0.06	0.51	0.54	0.38

mapping, EDX analysis (Fig. 3) confirmed that the synthesized N–CDs are composed of elements C, N, S, and O.

The synthesized NS-CDs present XRD patterns in Fig. 4 displaying a very intense broad peak around (2θ = 28.36°–28.56°) and a weak peak at (2θ = 40.30°–41.00°) corresponding to the (002) and (001) diffraction patterns of graphitic carbon [23]. From the Bragg's equation (Eq. (2)) the d-spacing value for synthesized N-CDs were calculated

$$n\lambda = 2d \operatorname{Sin} \theta (\text{ or}) \; d = n\lambda / 2 \operatorname{Sin} \theta \quad (2)$$

where, n is a positive integer (1), l is the wavelength of incident X-rays (λ = 1.54 Å) and q is the angle of plane. The d Inter planner distance calculated from NS-CDs are found in the C (002) plane around (3.144 nm; 3.122 nm; 3.155 nm; 3.121 nm; 3.120 nm) and in the C (100) plane around (4.411 nm; 4.511 nm; 4.421 nm; 4.295 nm; 4.451 nm). The following is also attached to Table 2 the results of some parameters of the NS-CDs sample.

Chemical composition of NS-CDs was determined by the Kjeldahl method for N and by XRF analysis for the other elements. As can be seen in Table 3, C, N, O, and S were found to be the major elements, while the others were in minority amounts. A similar chemical composition is usually found in NS-CDs as discussed in other references [24].

XPS survey was conducted to determine the chemical of the five NS-CDs (Fig. 5). The pronounced peaks at around 164 eV, 285 eV, 400 eV, and 531 eV correspond to S2p, C1s, N1s, and O1s, respectively [25]. The deconvolution of C1s surveys suggest three distinguish peaks including C═C/C–C (284.39 eV = NS-CDs 3:1, 284.49 eV = NS-CDs 2:1, 284.04 eV = NS-CDs 1:1, 283.85 eV = NS-CDs 1:2, 284.85 eV = NS-CDs 1:3), C–O/C–N (285.31 eV = NS-CDs 3:1, 285.32 eV = NS-CDs 2:1, 285.29 eV = NS-CDs 1:1, 285.21 eV = NS-CDs 1:2, 285.98 eV = NS-CDs 1:3) and C═O/C═N (287.71 eV = NS-CDs 3:1, 287.98 eV = NS-CDs 2:1, 287.53 eV = NS-CDs 1:1, 288.73 eV = NS-CDs 1:2, 287.98 eV = NS-CDs 1:3) for all the five NS-CDs **as shown in** Fig. 5(a **s/d e)-2** [26]. Their corresponding N1s high-resolution spectra can also be fitted into three peaks, which can be attributed to C–N–C (398.11 eV = NS-CDs 3:1, 400.23 eV = NS-CDs 2:1, 398.76 eV = NS-CDs 1:1, 400.10 eV = NS-CDs 1:2, 399.46 = NS-CDs 1:3), N–C (400.01 eV = NS-CDs 3:1, 401.66 eV = NS-CDs 2:1, 400.51 eV = NS-CDs 1:1, 402.23 eV = NS-CDs 1:2, 400.87 = NS-CDs 1:3), and N–H (402.56 eV = NS-CDs 3:1, 402.44 eV = NS-CDs 2:1, 401.40 eV = NS-CDs 1:1, 403.73 eV = NS-CDs 1:2, 401.88 = NS-CDs 1:3) for all the five NS-CDs as shown in Fig. 5(a s/d e)-3 [27]. Their corresponding O1s high-resolution spectra can also be fitted into three peaks, which can be attributed to C═O (530.23 eV = NS-CDs 3:1, 530.21 eV = NS-CDs 2:1, 530.13 eV = NS-CDs 1:1, 529.78 eV = NS-CDs 1:2, 530.61 = NS-CDs 1:3), C–O (531.56 eV = NS-CDs 3:1, 531.28 eV = NS-CDs 2:1, 531.50 eV = NS-CDs 1:1, 531.23 eV = NS-CDs 1:2, 531.93 = NS-CDs 1:3), and O═C–O (532.81 eV = NS-CDs 3:1, 532.70 eV = NS-CDs 2:1, 533.43 eV = NS-CDs 1:1, 532.73 eV = NS-CDs 1:2, 533.18 = NS-CDs 1:3) respectively, which were compatible with the characteristic C═O bond in the C1s spectrum as shown in Fig. 5(a s/d e)-4 [28]. The S2p peaks indicated the existence of three forms of Sulphur (S═O, $S2p^{1/2}$, and $S2p^{3/2}$), that is $S2p^{3/2}$ (163.01 eV = NS-CDs 3:1, 163.31 eV = NS-CDs 2:1, 163.13 eV = NS-CDs 1:1, 163.25 eV = NS-CDs 1:2, 163.53 = NS-CDs 1:3), $S2p^{1/2}$ (164.20 eV = NS-CDs 3:1, 164.45 eV = NS-CDs 2:1, 164.21 eV = NS-CDs 1:1, 164.96 eV = NS-CDs 1:2, 164.36 = NS-CDs 1:3), and S═O (165.41 eV = NS-CDs 3:1, 165.68 eV = NS-CDs 2:1, 165.86 eV = NS-CDs 1:1, 169.43 eV = NS-CDs 1:2, 164.76 = NS-CDs 1:3) as shown in Fig. 5(a s/d e)-1 [29]. Therefore, the functional groups of the asprepared NS-CDs characterized by XPS.

3.2. Optical characterization of synthesized NS–CDs

The optical characterization of NS-CDs was carried out by UV–visible spectroscopy, as shown in Fig. 6(a–b). The purpose of this analysis was to determine the absorbance ability and observe the changes in the band gap energy (Eg) of the synthesized samples. Fig. 6a shows that the NS-CDs material has a characteristic absorbance peak (205.99 nm = NS-CDs 3:1, 206.46 nm = NS-CDs 2:1, 206.94 = NS-CDs 1:1, 207.89 nm = NS-CDs 1:2, 207.91 nm = NS-CDs 1:3) at 350 nm in the UV light region and Eg = ~3.50 eV. And then N-CDs have absorbance peaks around at 260 nm, respectively, which are ascribed to the π-π* transition for the ring aromatic C═C bond in the carbon core [30], and the absorbance around at 340 nm is attributed to the transition n-π* [31] taking place between the C═O and C═N groups that collect on the surface and is only present on NS-CDs [32]. The change in the absorbance intensities and profile in N-CDs is hypothesized to be due to changes in the energy levels of the carbon dots after and before doped. The transition peaks confirm the formation of nitrogen and Sulphur functionalized CDs and these peaks are generated by CDs due to Mie scattering [33]. Fig. 6b shows that the samples had a decreased energy gap of 5.71 eV (NS-CDs 3:1), 5.46 eV (NS-CDs 3:1), 5.25 eV (NS-CDs 1:1), 5.51 eV (NS-CDs 1:2), and 5.56 eV (NS-CDs 1:3), As the doping concentration increases, the Fermi level shifts closer to the conduction band due to the increase in carrier concentration, carriers can be contributed by interstitial nitrogen and sulphur atoms or oxygen vacancies causing low energy intermediate transitions or inter band transitions to be prohibited and the band gap

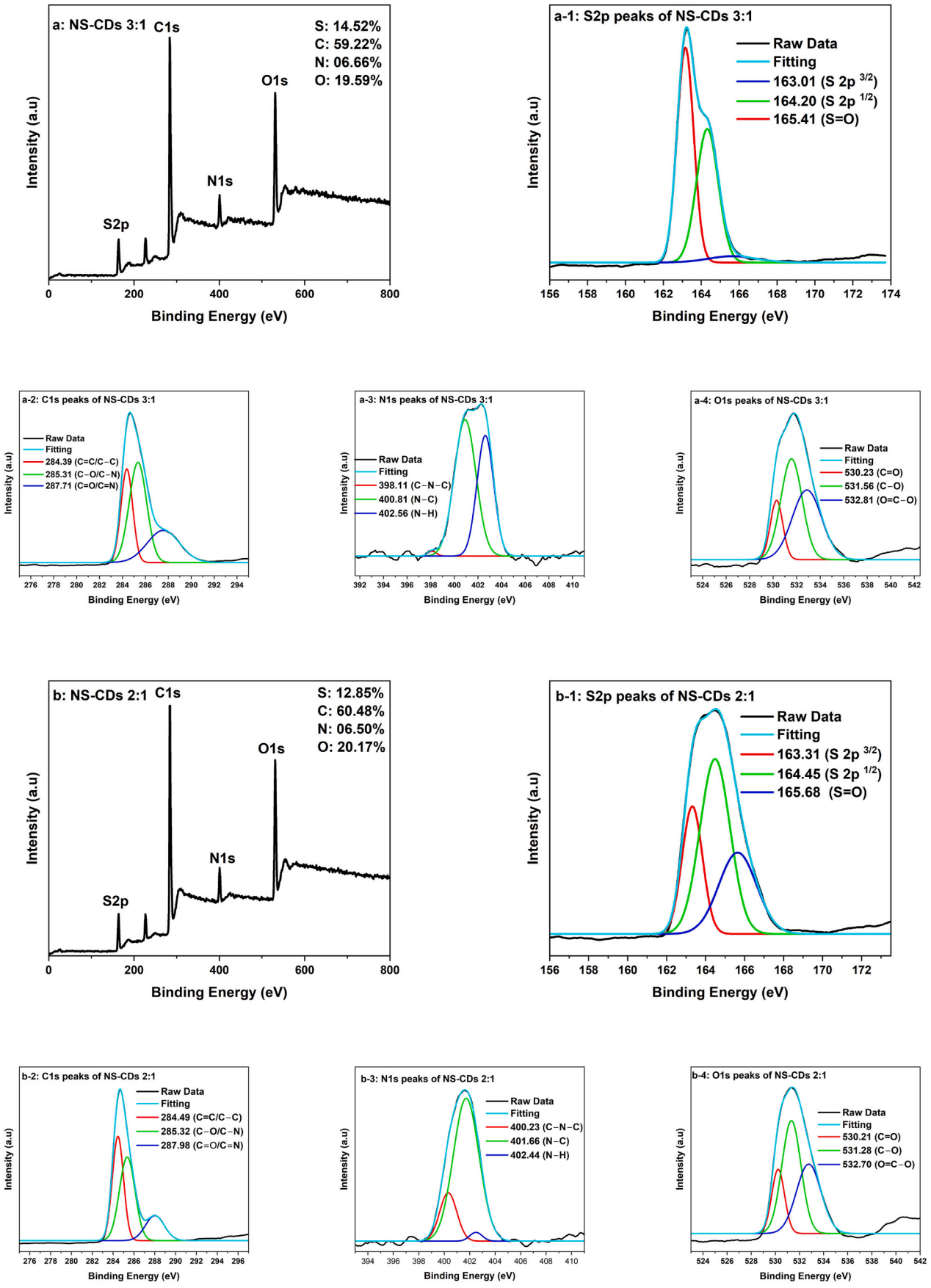

Fig. 5. XPS surveys of NS-CDs 3:1 (a), NS-CDs 2:1 (b) NS-CDs 1:1 (c), NS-CDs 1:2 (d), and NS-CDs 1:1 (e), S2p, C1s, N1s, O1s high resolution XPS surveys of NS-CDs 3:1 (a-1∼ a-4), NS-CDs 2:1 (b-1∼ b-4), NS-CDs 1:1 (c-1 ∼c-4), NS-CDs 1:2 (d-1∼ d-4), and NS-CDs 1:1 (e−1∼ e−4).

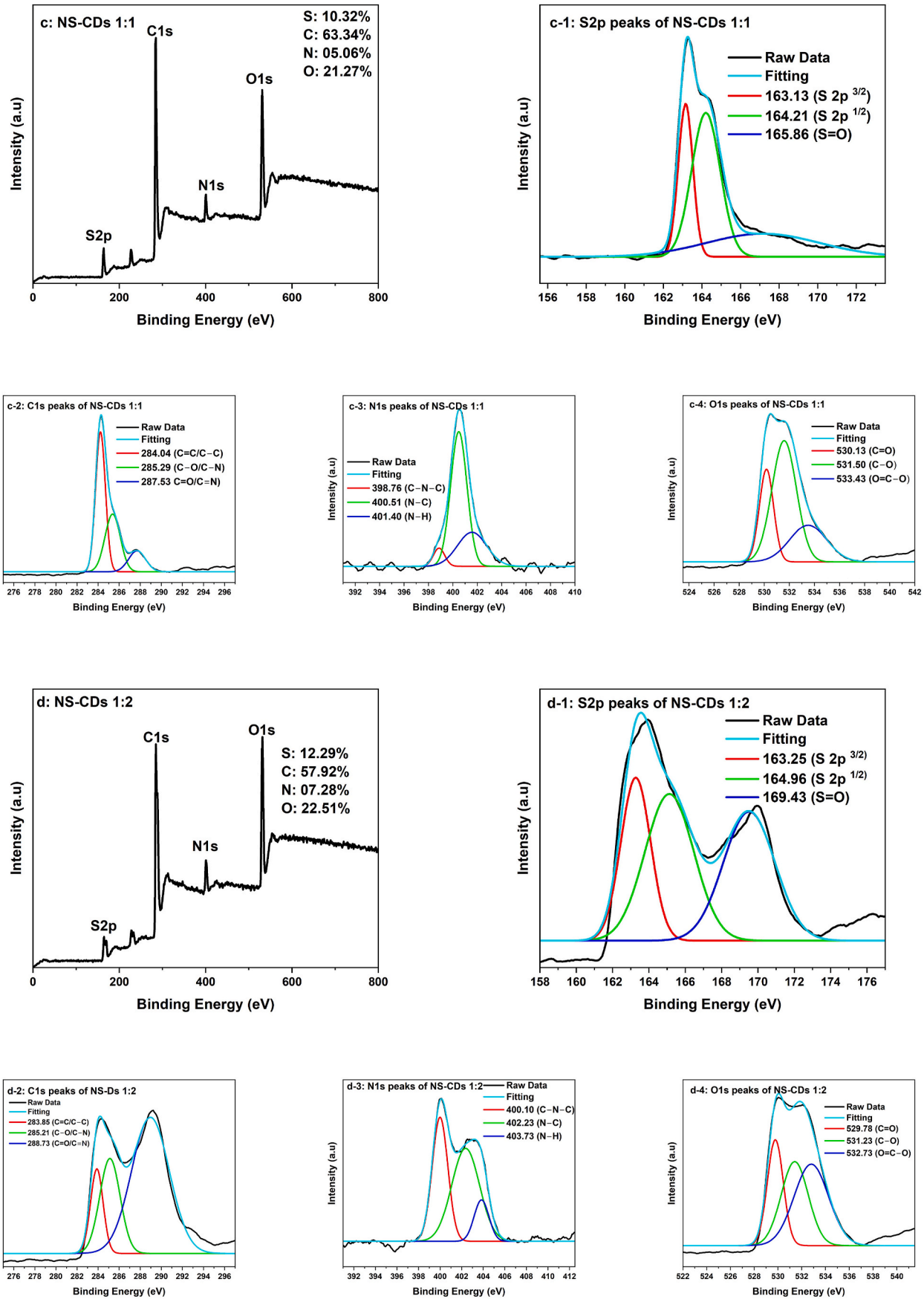

Fig. 5. (*continued*).

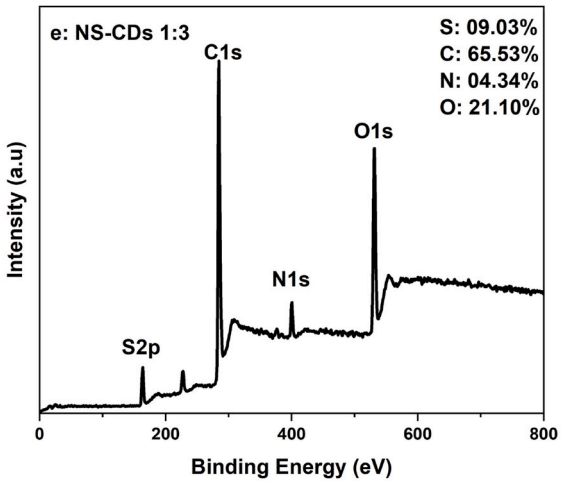

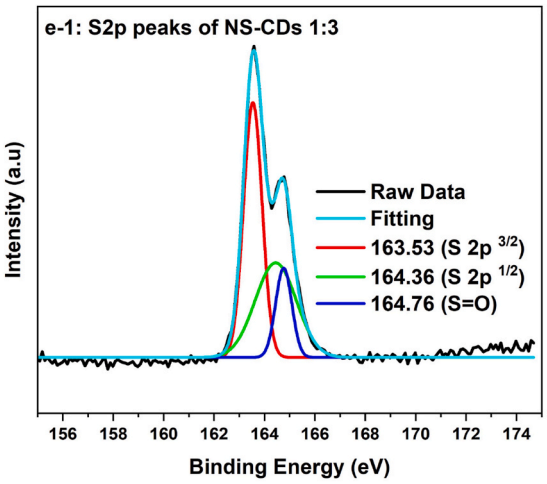

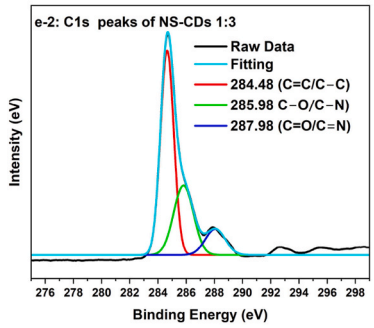

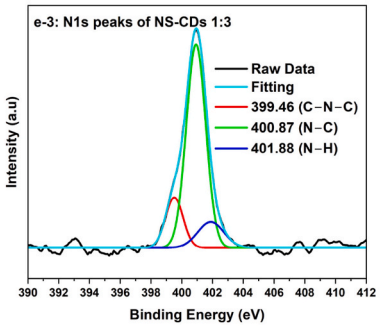

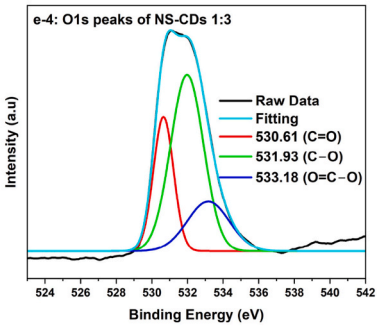

Fig. 5. (*continued*).

increases [34,35].

The photoluminescence spectrum of NS-CDs (3:1, 2:1, 1:1, 1:2, 1:3) particles in Fig. 6c showed, the presence of peak excitation at 403 nm and emission at 493.39 nm, 493.65 nm, 494.98 nm, 496.04 nm, and 497.11 nm, respectively. In this study, after there is a decrease in the PL intensity as the ratio of L-cysteine addition decreases, this is due to the decreased radiative recombination which shows high efficiency in separating (e^-/h^+) pairs that are needed in metal detection [36]. In this study, we introduce NS-CDs as a metal ion detector for Fe(III) and Pb(II). NS-CDs is one of the biosensor technologies that has been developed in various research fields, because of its environmentally friendly precursor source (agricultural biomass) and can be synthesized through environmentally friendly methods. Agricultural biomass has functional groups that are phenolic, carboxyl, ketone, aldehyde, and alcohol. These organic functional groups have the potential to become biosensor materials in detecting hazardous metals through several mechanisms. As seen in Fig. 6, the presence of NS-CDs has an effect on increasing the absorbance in the UV light region and also decreasing the PL intensity [37].

3.3. Mechanism of heavy metal ion detection

In this study, Atomic absorption spectroscopy (AAS) was used to detect metal content in Fe(III) and Pb(II) heavy metal ion solutions by adsorption method [38]. The following equation (Eq. (3)) and (Eq. (4)) will be used;

$$q = \frac{C_O - C_e}{W} \tag{3}$$

$$\%R = \frac{C_O - C_e}{C_O} \times 100\% \tag{4}$$

Where,

q = Adsorption capacity (mg/L)
Co = initial concentration (mg/L) = 10 mg/L.
Ce = Final concentration (mg/L)
W = mass of the adsorbent used in the experiment (g) = 0.2 mg.
R = Removal Efficiency (%)

From the equation (Eq. (3)) and (Eq. (4)), the results are shown in Table 4. The results obtained in the NS-CDs 1:3 sample had the best Fe (III) and Pb (II) heavy metal absorption rates with Fe (III), namely Adsorption capacity worth 21.35 mg/L and Removal Efficiency worth 85.40 %. Then for Pb (II), the Adsorption capacity is 24.60 mg/L and Removal Efficiency is 98.40 %. With the higher the adsorption rate of heavy metals obtained in the material, the better the detection ability of these heavy metals. The results produced are expected to help overcome problems, especially related to the environment and waste treatment [39].

AAS testing was used to evaluate the ability of NS-CDs to detect Fe (III) and Pb(II) heavy metal ions. NS-CDs contain functional groups sensitive to Fe(III) and Pb(II) ions such as –OH, and $–NH_2$, on the surface, which will lead to the formation of nonfluorescent complexes [40]. The evaluated metal ions might participate in limiting fluorescence quenching due to their interaction with electron donor groups present on NS-CDs. In general, fluorescence quenching of NS-CDs resulted from dynamic quenching (electron transfer process) or static quenching (formation of non-fluorescent complexes). The fluorescence quenching

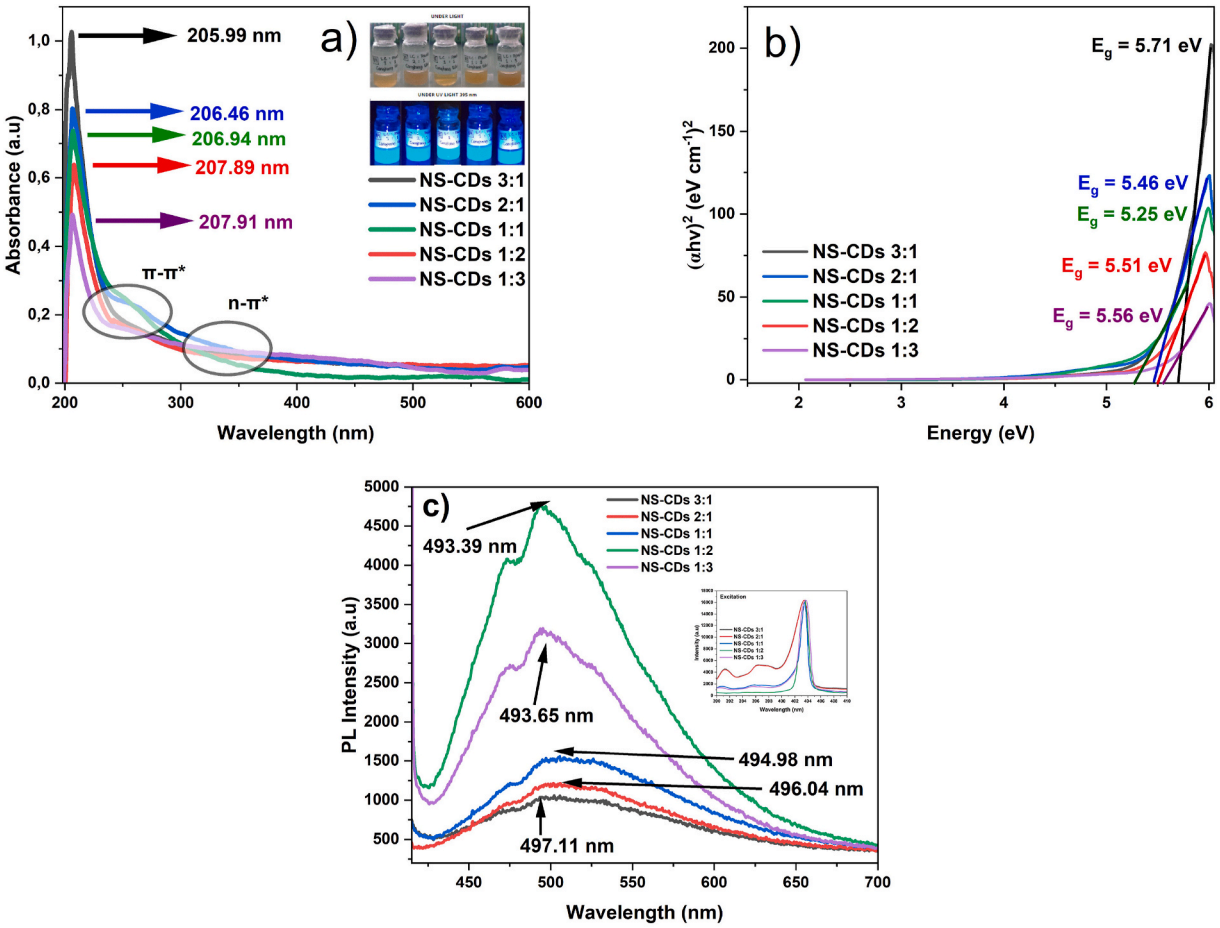

Fig. 6. UV–vis absorption spectra (a), (αhν) [2] versus energy curve (b), comparisons of fluorescence spectra of NS-CDs (c).

Table 4
Calculation of the formula Heavy Metal Ion Detection Study.

Sample	Parameter	Ce (mg/L)	q (mg/L)	R (%)	relative standard deviation (%)
NS-CDs 3:1	Fe(III)	2.82	10.90	43,60	0.192
	Pb(II)	0.26	23.70	94,80	0.013
NS-CDs 2:1	Fe(III)	2.74	11.30	45,20	0.011
	Pb(II)	0.25	23.75	95,00	0.049
NS-CDs 1:1	Fe(III)	1.27	18.65	74,60	0.003
	Pb(II)	0.23	23.85	95,40	0.024
NS-CDs 1:2	Fe(III)	0.91	20.45	81,80	0.005
	Pb(II)	0.18	24.10	96,40	0.010
NS-CDs 1:3	Fe(III)	0.73	21.35	85,40	0.004
	Pb(II)	0.08	24.60	98,40	0.010

process is evidenced by the adsorption of metal ions on the NS-CDs. This results in intermolecular interactions so as to detect heavy metal ions Fe (III) and Pb(II) can be adsorbed properly as shown in Table 4 [41].

4. Conclusion

The heavy metal detection material, namely NS-CDs with variations of Cavendish Banana Peel and L-Cysteine precursors (3:1, 2:1, 1:1, 1:2, 1:3), has been successfully synthesized using the solvothermal method. Subsequently, characterization was performed using HR-TEM, EDX, XPS, XRF, XRD, UV–Vis, PL, along with heavy metal ion detection testing using AAS. In HR-TEM testing, the average particle sizes of NS-CDs 3:1, 2:1, 1:1, 1:2, 1:3 were confirmed to be 1.19 nm; 1.02 nm; 1.17 nm; 1.28 nm; 1.35 nm respectively, with a lattice spacing of 0.28 nm. Furthermore, it has been confirmed using EDX and XRF that carbon (C), nitrogen (N), Sulphur (S), and oxygen (O) are the main elements in this material. XRD testing yielded interplanar distances of NS-CDs 3:1, 2:1, 1:1, 1:2, 1:3 respectively on the C (002) plane around (3.144 nm; 3.122 nm; 3.155 nm; 3.121 nm; 3.120 nm) and in the C (100) plane around (4.411 nm; 4.511 nm; 4.421 nm; 4.295 nm; 4.451 nm). Next, in XPS testing, S2p, C1s, N1s, and O1s peaks correlated around 64 eV, 285 eV, 400 eV, and 531 eV respectively. In UV–Vis testing, the absorbance peaks were (205.99 nm = NS-CDs 3:1, 206.46 nm = NS-CDs 2:1, 206.94 = NS-CDs 1:1, 207.89 nm = NS-CDs 1:2, 207.91 nm = NS-CDs 1:3). Then, in PL testing for NS-CDs 3:1, 2:1, 1:1, 1:2, 1:3, the spectrum showed peak excitation at 403 nm and emission at 493.39 nm, 493.65 nm, 494.98 nm, 496.04 nm, and 497.11 nm, respectively. Furthermore, in the trial phase to detect Fe(III) and Pb(II) heavy metal ions with AAS, it was found that each sample could absorb heavy metals well, especially in the NS-CDs 1:3 sample with Adsorption capacity worth 21.35 mg/L and Removal Efficiency worth 85.40 %. Based on the test results presented, NS-CDs material made using Cavendish Banana Peel has good adsorption for further heavy metal detection studies.

CRediT authorship contribution statement

Muhammadin Hamid: Conceptualization. **Syahrul Humaidi:** Investigation. **Hadi Wijoyo:** Methodology. **Isnaeni Isnaeni:** Project administration. **Indah Revita Saragi:** Resources. **Crystina Simanjuntak:** Software. **Noor Haida Mohd Kaus:** Validation. **M.M.A. Kechik:** Writing – original draft, Conceptualization. **Agus Nurbillah:** Data curation. **Yazid Yaakob:** Data curation. **Tulus Ikhsan Nasution:** Investigation.

Declaration of competing interest

The authors declare that they have no known competing financial interests or personal relationships that could have appeared to influence the work reported in this paper.

Data availability

Data will be made available on request.

Acknowledgement

The authors would like to thank the Universitas Sumatera Utara for the TALENTA Universitas Sumatera Utara with scheme government collaboration and contract number 13388/UN5.1.R/PPM/2023.

References

[1] P.M. Godwin, Y. Pan, H. Xiao, M.T. Afzal, Progress in preparation and application of Modified Biochar for Improving heavy metal ion Removal from wastewater, J. Bioresour. Bioprod. 4 (1) (2019) 31–42, https://doi.org/10.21967/jbb.v4i1.180.

[2] C.L. Ekeanyanwu, C.S. Alisi, R.C. Ekeanyanwu, Levels of Aflatoxin M1 and selected heavy metals (Pb, Cd, Cr, Cu, Zn, Fe, as, and Hg) in the breast milk of lactating mothers in South Eastern, Nigeria, Food Control 112 (November 2019) (2020) 107150, https://doi.org/10.1016/j.foodcont.2020.107150.

[3] Y. Zhu, X. Wang, P. Wang, J. Zhu, Y. He, X. Jia, F. Chang, H. Wang, G. Hu, Two-dimensional BCN nanosheets self-assembled with hematite nanocrystals for sensitively detecting trace toxic Pb(II) ions in natural water, Ecotoxicol. Environ. Saf. 225 (2021) 112745, https://doi.org/10.1016/j.ecoenv.2021.112745.

[4] S. Chen, Y. Hao, S. Liu, Y. Liu, Z. Zhang, M. Fang, L. Geng, Boron and nitrogen Co-doped carbon dots as the dual functional fluorescent probe for Fe3+ and PH detection, J. Saudi Chem. Soc. 28 (1) (2024) 101775, https://doi.org/10.1016/j.jscs.2023.101775.

[5] L.J. Mohammed, K.M. Omer, Dual functional highly Luminescence B, N Co-doped carbon Nanodots as Nanothermometer and Fe3+/Fe2+ sensor, Sci. Rep. 10 (1) (2020) 1–12, https://doi.org/10.1038/s41598-020-59958-5.

[6] D.A. Barus, R.T. Ginting, A. Faizah, R. Shafira, K. Nainggolan, Carbon dots synthesis from soybean with urea doped as sensitive Fe(II) ion detection, Indones. J. Chem. Res. 10 (3) (2023) 171–176, https://doi.org/10.30598//ijcr.

[7] H. Liu, Y. Zhang, C. Huang, Development of nitrogen and sulfur-doped carbon dots for cellular imaging, J. Pharm. Anal. 9 (2) (2019) 127–132, https://doi.org/10.1016/j.jpha.2018.10.001.

[8] M. Hamid, S. Humaidi, I.R. Saragi, C. Simanjuntak, I. Isnaeni, H. Wijoyo, The effectiveness of activated carbon from nutmeg shell in reducing ammonia (NH3) levels in fish pond water, Carbon Trends 14 (January 2024) (2024) 1–12.

[9] K. Daphne Jacinth Gracia, R. Muthukumar Sivaraman, S. Sheeba Thavamani, T. Peter Amaladhas, S. Devanesan, M.S. AlSalhi, M. Balakrishnan, Nitrogen doped fluorescent carbon dots from delonix regia for Fe(III) and cysteine sensing, DNA binding and bioimaging, Arab. J. Chem. 16 (10) (2023) 105109, https://doi.org/10.1016/j.arabjc.2023.105109.

[10] M. Hamid, Susilawati, S.A. Amaturrahim, I.B. Dalimunthe, A. Daulay, Synthesis of magnetic activated carbon-supported cobalt(II) chloride derived from pecan shell (Aleurites moluccana) with Co-precipitation method as the electrode in supercapacitors, Mater. Sci. Energy Technol. 6 (2023) 429–436, https://doi.org/10.1016/j.mset.2023.04.004.

[11] D. Savitri, K. Djawad, M. Hatta, S. Wahyuni, A. Bukhari, Active compounds in kepok banana peel as anti-inflammatory in acne vulgaris: review article, Ann. Med. Surg. 84 (August) (2022) 104868, https://doi.org/10.1016/j.amsu.2022.104868.

[12] M.R. Islam, M.M. Kamal, M.R. Kabir, M.M. Hasan, A.R. Haque, S.M.K. Hasan, Phenolic compounds and antioxidants activity of banana peel extracts: testing and optimization of enzyme-assisted conditions, Meas. Food 10 (March) (2023) 100085, https://doi.org/10.1016/j.meafoo.2023.100085.

[13] K.M. Lavanya, J.A.K. Florence, B. Vivekanandan, R. Lakshmipathy, Comparative investigations of raw and alkali metal free banana peel as adsorbent for the removal of Hg2+ions, Mater. Today Proc. 55 (xxxx) (2021) 321–326, https://doi.org/10.1016/j.matpr.2021.07.410.

[14] C.W. Hsieh, R.K. Singh, S. Som, C.H. Lu, Detection of Fe (III) using APTES-coated CsPbBr3–CsPb2Br5 perovskite quantum dots, Chem. Eng. J. Adv. 12 (July) (2022), https://doi.org/10.1016/j.ceja.2022.100358.

[15] K.A. Abdalkarim, S.B. Aziz, R.T. Abdulwahid, S.M. Alshehri, T. Ahamad, J.M. Hadi, S.A. Hussein, Synthesis of Hg metal complex and its application to reduce the optical band gap of polymer, Arab. J. Chem. 14 (7) (2021) 103215, https://doi.org/10.1016/j.arabjc.2021.103215.

[16] M. Hamid, T.I. Nasution, S. Syafrina, I. Isnaeni, Synthesis and characterization of ruminant feed based on palm kernel cake using EM4 fermentation method, IOP Conf. Ser. Earth Environ. Sci. 1352 (1) (2024), https://doi.org/10.1088/1755-1315/1352/1/012097.

[17] M. Hamid, T.I. Nasution, I.I. Putriana, Synthesis and characterization of Indigofera zollingeriana plant-based ruminant feed using EM 4 fermentation method synthesis and characterization of Indigofera zollingeriana plant-based ruminant feed using EM 4 fermentation method, IOP Conf. Ser. Earth Environ. Sci. (2024), https://doi.org/10.1088/1755-1315/1352/1/012098.

[18] Z. Yi, X. Li, H. Zhang, X. Ji, W. Sun, Y. Yu, Y. Liu, J. Huang, Z. Sarshar, M. Sain, High quantum yield photoluminescent N-doped carbon dots for switch sensing and imaging, Talanta 222 (July 2020) (2021) 121663, https://doi.org/10.1016/j.talanta.2020.121663.

[19] S. Humaidi, M. Hamid, H. Wijoyo, Study and characterization of BaFe12O19/PVDF composites as electrode materials for supercapacitors, Biosens. Bioelectron. X 19 (June) (2024) 100507, https://doi.org/10.1016/j.biosx.2024.100507.

[20] D.G. Ayu, S. Gea, N. Andriayani, D.J. Telaumbanua, A.F.R. Piliang, M. Harahap, Z. Yen, R. Goei, A.I.Y. Tok, Photocatalytic degradation of methylene blue using N-doped ZnO/carbon dot (N-ZnO/CD) nanocomposites derived from organic soybean, ACS Omega 8 (17) (2023) 14965–14984, https://doi.org/10.1021/acsomega.2c07546.

[21] S.D. Torres Landa, N.K. Reddy Bogireddy, I. Kaur, V. Batra, V. Agarwal, Heavy metal ion detection using green precursor derived carbon dots, iScience 25 (2) (2022) 103816, https://doi.org/10.1016/j.isci.2022.103816.

[22] Z. Wang, D. Chen, B. Gu, B. Gao, T. Wang, Q. Guo, G. Wang, Biomass-derived nitrogen doped graphene quantum dots with color-tunable emission for sensing, fluorescence ink and multicolor cell imaging, Spectrochim. Acta Part A Mol. Biomol. Spectrosc. 227 (2020) 117671, https://doi.org/10.1016/j.saa.2019.117671.

[23] V. Arul, M.G. Sethuraman, Facile green synthesis of fluorescent N-doped carbon dots from actinidia deliciosa and their catalytic activity and cytotoxicity applications, Opt. Mater. 78 (2018) 181–190, https://doi.org/10.1016/j.optmat.2018.02.029.

[24] S.S. Monte-Filho, S.I.E. Andrade, M.B. Lima, M.C.U. Araujo, Synthesis of highly fluorescent carbon dots from lemon and onion juices for determination of riboflavin in multivitamin/mineral supplements, J. Pharm. Anal. 9 (3) (2019) 209–216, https://doi.org/10.1016/j.jpha.2019.02.003.

[25] H. Wang, P. Gao, Y. Wang, J. Guo, K.Q. Zhang, D. Du, X. Dai, G. Zou, Fluorescently tuned nitrogen-doped carbon dots from carbon source with different content of carboxyl groups, Apl. Mater. 3 (8) (2015) 1–8, https://doi.org/10.1063/1.4928028.

[26] M. Lavkush Bhaisare, S. Pandey, M. Shahnawaz Khan, A. Talib, H.F. Wu, Fluorophotometric determination of critical micelle concentration (CMC) of ionic and non-ionic surfactants with carbon dots via Stokes shift, Talanta 132 (Cmc) (2015) 572–578, https://doi.org/10.1016/j.talanta.2014.09.011.

[27] X. Liao, C. Chen, R. Zhou, Q. Huang, Q. Liang, Z. Huang, Y. Zhang, H. Hu, Y. Liang, Comparison of N-doped carbon dots synthesized from the main components of plants including cellulose, lignin, and xylose: characterized, fluorescence mechanism, and potential applications, Dye. Pigment. 183 (May) (2020) 108725, https://doi.org/10.1016/j.dyepig.2020.108725.

[28] K. Nakason, B. Panyapinyopol, V. Kanokkantapong, N. Viriya-empikul, W. Kraithong, P. Pavasant, Characteristics of hydrochar and liquid fraction from hydrothermal carbonization of cassava rhizome, J. Energy Inst. 91 (2) (2018) 184–193, https://doi.org/10.1016/j.joei.2017.01.002.

[29] S. Mohandoss, S. Palanisamy, V.V. Priya, S.K. Mohan, J.-J. Shim, K. Yelithao, S. You, Y.R. Lee, Excitation-dependent multiple luminescence emission of nitrogen and sulfur Co-doped carbon dots for cysteine sensing, bioimaging, and photoluminescent ink applications, Microchem. J. 167 (April) (2021) 106280, https://doi.org/10.1016/j.microc.2021.106280.

[30] H. Qi, M. Teng, M. Liu, S. Liu, J. Li, H. Yu, C. Teng, Z. Huang, H. Liu, Q. Shao, A. Umar, T. Ding, Q. Gao, Z. Guo, Biomass-derived nitrogen-doped carbon quantum dots: highly selective fluorescent probe for detecting Fe 3+ ions and tetracyclines, J. Colloid Interface Sci. 539 (2019) 332–341, https://doi.org/10.1016/j.jcis.2018.12.047.

[31] C. Kan, X. Shao, F. Song, J. Xu, J. Zhu, L. Du, Bioimaging of a fluorescence rhodamine-based probe for reversible detection of Hg (II) and its application in real water environment, Microchem. J. 150 (July) (2019) 104142, https://doi.org/10.1016/j.microc.2019.104142.

[32] Y. Wang, X. Hu, W. Li, X. Huang, Z. Li, W. Zhang, X. Zhang, X. Zou, J. Shi, Preparation of boron nitrogen Co-doped carbon quantum dots for rapid detection of Cr(VI), Spectrochim. Acta Part A Mol. Biomol. Spectrosc. 243 (2020) 118807, https://doi.org/10.1016/j.saa.2020.118807.

[33] S. Qu, X. Wang, Q. Lu, X. Liu, L. Wang, A biocompatible fluorescent ink based on water-soluble luminescent carbon nanodots, Angew. Chemie - Int. Ed. 51 (49) (2012) 12215–12218, https://doi.org/10.1002/anie.201206791.

[34] A. Sasinska, D. Bialuschewski, M.M. Islam, T. Singh, M. Deo, S. Mathur, Experimental and theoretical insights into influence of hydrogen and nitrogen plasma on the water splitting performance of ALD grown TiO2 thin films, J. Phys. Chem. C 121 (29) (2017) 15538–15548, https://doi.org/10.1021/acs.jpcc.7b03424.

[35] J. Sahu, S. Soni, S. Kumar, B. Dalela, P.A. Alvi, S.S. Sharma, D.M. Phase, M. Gupta, S. Kumar, S. Dalela, Defects and oxygen vacancies tailored structural, optical and electronic structure properties of Co-doped ZnO nanoparticle samples probed using soft X-ray absorption spectroscopy, Vacuum 179 (June) (2020), https://doi.org/10.1016/j.vacuum.2020.109538.

[36] B. Wang, X. Wang, L. Lu, C. Zhou, Z. Xin, J. Wang, X.K. Ke, G. Sheng, S. Yan, Z. Zou, Oxygen-vacancy-activated CO2 splitting over amorphous oxide semiconductor photocatalyst, ACS Catal. 8 (1) (2018) 516–525, https://doi.org/10.1021/acscatal.7b02952.

[37] A.S. Prayugo, Marpongahtun, S. Gea, A. Daulay, M. Harahap, J. Siow, R. Goei, A.I. Y. Tok, Highly fluorescent nitrogen-doped carbon dots derived from jengkol peels (archindendron pauciflorum) by solvothermal synthesis for sensitive Hg2+ ions

detection, Biosens. Bioelectron. X 14 (1) (2023) 100363, https://doi.org/10.1016/j.biosx.2023.100363.

[38] M. Rianna, A. Talanda, Y. Pratama, S. Humaidi, E.A. Setiadi, A.P. Tetuko, L. F. Nurdiyansah, T. Sembiring, P. Sebayang, Evaluation of Co0.7Ni0.3Fe2O4 nanoparticle on structural, morphological, and magnetic properties as a heavy metal adsorbent in Cu, Cr, Mater. Sci. Energy Technol. 6 (2023) 77–80, https://doi.org/10.1016/j.mset.2022.11.011.

[39] H. Ebrahimzadeh, M. Behbahani, A novel lead imprinted polymer as the selective solid phase for extraction and trace detection of lead ions by flame atomic absorption spectrophotometry: synthesis, characterization and analytical application, Arab. J. Chem. 10 (2017) S2499–S2508, https://doi.org/10.1016/j.arabjc.2013.09.017.

[40] X. Xu, R. Ray, Y. Gu, H.J. Ploehn, L. Gearheart, K. Raker, W.A. Scrivens, Electrophoretic analysis and purification of fluorescent single-walled carbon nanotube fragments, J. Am. Chem. Soc. 126 (40) (2004) 12736–12737, https://doi.org/10.1021/ja040082h.

[41] R. Xie, Y. Qu, M. Tang, J. Zhao, S. Chua, T. Li, F. Zhang, H. E, A. Wheatley, F. Chai, Carbon dots-magnetic nanocomposites for the detection and removal of Hg2+, Food Chem. 364 (June) (2021) 130366 https://doi.org/10.1016/j.foodchem.2021.130366.